# A Three-Dimensional Modeling Analysis of CANDU 9 End-Shield Cooling Effects with CFX-4 Code: Preliminary Results

Y. Zhuang, A.O. Banas and R.Q.N. Zhou

**Abstract**

End-shield cooling effects in CANDU 9 under both normal and accidental conditions have been analyzed, using a commercial three-dimensional code, CFX-4. The simulated three-dimensional heat transfer agrees with the design specifications for normal operation conditions. In the event of loss of forced flow, the code predicts a maximum temperature of 96$^0$C on the fueling tubesheet, which is far below the coolant boiling point of 143$^0$C. The detailed temperature distribution in the end shield, simulated with the code, can be used as input for stress analysis.

## 1. Introduction

Analysis of end-shield cooling failures is a safety requirement for CANDU 9 reactors. The concern is that the heatup of end shields resulting from a loss of cooling can cause thermal stress, which in turn could result in damage to the calandria and possibly in fuel channel failures.

CANDU 9 end shields have a complex configuration, consisting of tubesheets, lattice tubes, and space filled with shielding balls and demineralized water. Knowledge of local maximum temperatures in the individual end-shield components is necessary for thermal stress analysis. Existing modeling analysis (Popov 1997) using a one-dimensional code could not capture the three-dimensional nature of the flow structure and heat transfer in the end shields, and results from it need to be confirmed independently by a more detailed model study.

Even with a three-dimensional code, it is impossible to model the end-shield flow structure and heat transfer in every detail. Therefore, a porous medium approximation is implemented in CFX-4 to account for the hydraulic resistance of the lattice tubes and steel balls (or solid matrix) exerted on the flow. This, however, gives rise to the problem of modeling heat transfer within a porous medium and between a wall and the porous medium.

In this paper, we briefly discuss our treatments of heat transfer within a porous medium and between a wall and the porous medium in CFX-4, and then present a preliminary numerical investigation of the end-shield cooling effects. The essential features of this study are: (1) the three-dimensional end-shield effects are simulated with little approximation, (2) heat sources in both liquid and metal components, and their spatial distribution are readily incorporated in the code, and (3) the three-dimensional distribution of the temperature is predicted, allowing for the location of hot spots and the dominant local temperature gradients.

## 2. Heat transfer within a porous medium

The common method of predicting heat transfer in a porous medium is to use an effective thermal conductivity, $\lambda_e$, and an interstitial heat transfer coefficient, $h_{sf}$, in the energy equation for the porous medium:

$$\rho_s C_{ps} \frac{\partial T_s}{\partial t} = \nabla \bullet (\lambda_e \nabla T_s) + A_0 h_{sf} (T_f - T_s) + Q_s \quad , \qquad (1)$$

where $\rho_s$ is the density of the solid matrix, $C_{ps}$ is the specific heat, $T_s$ and $T_f$ are the temperatures of the solid matrix and the fluid, respectively, $A_0$ is the specific interfacial area, and $Q_s$ is the heat source per unit porous volume.

Eq. (1) indicates that the local temperature in the solid matrix depends on conduction (first term), heat exchange between the liquid and the solid matrix (second term), and the local heat source. An earlier study (Zhou and Banas 1996) has shown that the CFX-4 code has difficulties in obtaining a well-converged solution for a small effective thermal conductivity ($\lambda_e = 3.71$ W m$^{-1}$K$^{-1}$). Fortunately, Eq. (1) can be simplified in the current study. A simple order-of-magnitude analysis of Eq. (1) shows that the interstitial heat transfer and source terms on the right-hand side of the equation are about 3 to 4 orders of magnitude higher than the conduction term. Thus, for practical applications, we can safely neglect the conduction term in Eq. (1). This not only solved the convergence problem in the CFX-4, but also resulted in a significant decrease in computing time, since Eq. (1) could now be implemented through the user FORTRAN in CFX-4.

## 3. Heat transfer between a wall and the adjacent porous media

Currently, there is no special treatment of heat transfer between the wall and fluid in CFX-4 when a porous medium is modeled. When the turbulence k-ε model is used, CFX-4 calculates flow and heat transfer in the near-wall region with their respective wall functions, instead of using an extremely fine grid to account for the rapid variations of the flow quantities. The wall function for heat transfer **implicitly** assumes a wall heat-transfer coefficient (CFX-4 user guide 1996):

$$h_w = \frac{\rho C_\mu^{1/2} k^{1/2} C_p}{\Pr y^+} \quad , \qquad (2)$$

where $\rho$ is the density of the fluid, $C_\mu$ is a constant equal to 0.09, $k$ is the turbulent kinetic energy, $C_{p.}$ is the specific heat of the fluid, Pr is the Prandtl number, and $y^+$ is a dimensionless quantity measuring the distance from the wall, ranging from 30 to 100.

Applying Eq. (2) to a porous wall region is inadequate. This is because the direct contact between the porous media and the wall has changed the structure of the normal boundary layer. Eq. (2) is derived from the normal wall function in the absence of a porous medium, and is unlikely to be still valid. In fact, the presence of a porous medium gives rise to the transverse migration, or dispersion of the fluid particles from the parallel lines they would have followed in the absence of the porous medium. This extra mixing of the fluid particles increases heat transfer between the wall and the porous medium. Eq. (2) does not take this extra heat-transfer effect into consideration.

Another factor that complicates flow and heat transfer in the vicinity of a wall is the variation of porosity in that region. For a packed bed of spheres, the porosity is larger and thence hydraulic resistance is lower near the wall, resulting in an increase in local velocity and the Reynolds number. This has been referred to as a channeling effect. It has been suggested that it is important to model the channeling effect when the primary heat transfer is through the wall surfaces (Kaviany 1995).

The functional dependence of the porosity on the distance from the wall, which has been studied in a number of experiments, can be represented very well by an exponential function:

$$\gamma = \gamma_0 (1 + b\exp(-\frac{cy}{d_p})) \quad , \qquad (3)$$

where $\gamma_0$ is the uniform porosity far from the wall, and $d_p$ is the diameter of the sphere. The empirical constants $b$ and $c$ are determined from experiments.

## 4. Implementation of heat transfer between a wall and the adjacent porous medium in CFX-4

Since there is no equivalent wall function to Eq. (2) that has been proposed to date, we have decided to replace Eq. (2) with a validated wall heat-transfer coefficient (Yagi and Wakao 1959) in CFX-4:

$$\frac{h_w d_p}{k_f} = \begin{cases} 0.6\,\mathrm{Pr}^{1/3}\,\mathrm{Re}^{1/2} & 1 < \mathrm{Re} \le 40 \\ 0.2\mathrm{Pr}^{1/3}\,\mathrm{Re}^{0.8} & 40 < \mathrm{Re} \le 2000 \end{cases} \quad , \qquad (4)$$

where $k_f$ is the thermal conductivity of the fluid, and Re is the Reynolds number based on the diameter of the steel balls. It is believed that Eq. (4) is more accurate for the Reynolds number between 40 and 2000 (Dixon and Cresswell 1979). This applies to the present analysis, where the typical Re is of the order of a few hundred. Eq. (4) also gives smaller value when compared with other correlations (Dixon and Cresswell 1979), and thus is more conservative for the present analysis.

Eq. (4) is implemented in CFX-4 through a user FORTRAN program, USRWTM, which replaces the default heat-transfer coefficient defined by Eq. (2) with Eq. (4).

Since it has been shown that the effect of the frictional resistance on flow structure is insignificant, the wall function for the flow is not changed. However, the variation of porosity in the near-wall region is modeled in the CFX-4 using Eq. (3) to account for the channeling effect, which has a direct impact on the heat-transfer rate.

## 5. Model calculations

CFX-4 is used to model the flow and heat transfer in the end shield, assuming a constant porosity of 0.25, except in the near-wall region, where the variation of the porosity follows Eq. (3). The end shield is discretized into a mesh of 52512 nodes by the CFX meshbuild utility. The flow is assumed to enter from the bottom, and exit from the top of the end shield. The inlet and outlet are specified as mass flow and pressure boundary conditions, respectively.

The reactor is assumed to be at full power for all the model calculations. The total heat generated by nuclear radiation in a single end shield is 3.4 MW. This does not include 30% contingency to cover the uncertainty in the estimate of the heat balance (Smith 1995). The heat is assumed to be deposited uniformly in the water (1.02 MW), solid matrix of steel balls and lattice tubes (1.98 MW), and moderator-side tubesheet (0.4 MW). There is no heat generation in the fueling tubesheet.

The end shield also exchanges heat with the tubesheets on both fueling machine and moderator sides. The boundary conditions on the outsides of the tubesheets are specified by a constant air temperature (288°C) on the fueling machine side, and a constant water temperature (70°C) on the moderator side. The heat-transfer coefficients are 14 $Wm^{-2}K^{-1}$ for the air, and 1067 $Wm^{-2}K^{-1}$ for the water (Zhou and Banas 1996).

Model simulations under both normal operation and loss-of-forced-flow conditions have been performed. Only steady-state cases are reported here.

### 5.1 Normal operation condition

Under normal operation condition, the inlet fluid temperature is 40°C and the flow rate is 98 kg $s^{-1}$. With the improved heat transfer, the model predicts a wall heat-transfer coefficient varying from 2132 $Wm^{-2}K^{-1}$ in the middle to 2395 $Wm^{-2}K^{-1}$ at the bottom and the top of the end shield.

The model calculations of coolant and tubesheet temperature distributions are presented in Fig. 1. It can seen in Fig. 1(a) that the fluid temperature rises approximately 11°C through the end shield. Substituting this temperature difference into the energy balance equation

$$E_{in} = \dot{m} C_p (T_{outlet} - T_{inlet}), \qquad (5)$$

where $\dot{m}$ is the flow rate and $C_p$ is the specific heat of the fluid, we obtain the total input energy to the end shield, $E_{in}$ = 4.53 MW. Thus the heat the cooling fluid received from the tubesheets is 1.13 MW (=$E_{in}$ - 3.4 MW), which represents about 25% of the total input energy.

Temperature distributions in the tubesheets, with the nearby cooling flow velocities superimposed, are shown in Figs. 1 (b,c). It can be seen that the tubesheet on the moderator side is hotter and the temperature is more uniform than the tubesheet on the fueling side. This is caused by the nuclear heating inside the tubesheet on the moderator side. A maximum temperature of 64°C is predicted at the top on the moderator tubesheet.

Owing to the presence of the porous media, and its high hydraulic resistance, the flow pattern inside the end shield becomes fairly uniform. It is therefore unlikely to result in any local hot spot, given a uniform heat-source distribution.

5.2 Loss-of-forced-flow condition

Under loss-of-forced-flow condition, we assume that the heat exchanger is still operating so that the inlet fluid temperature remains at 40°C. The 30 kg $s^{-1}$ thermosyphoning flow rate predicted by CATHENA (Popov 1997) is assumed for inlet flow.

As expected, when the flow rate decreases, the code calculates a smaller wall heat-transfer coefficient, varying from 900 $Wm^{-2}K^{-1}$ to 980 $Wm^{-2}K^{-1}$, which means that less heat will be transferred to the cooling fluid from the tubesheets. However, the decreased flow rate and the constant radiation heat deposition rate inside the end shield result in a large increase in the outlet fluid temperature. Figure 2 (a) shows that the temperature difference between the outlet and the inlet is about 33°C. Performing a similar calculation as done for normal operation condition, using Eq. (5), we obtain the total input energy $E_{in}$ = 4.15 MW, which implies that the heat from the tubesheets is 4.15 - 3.4 = 0.75 MW.

Similar to the normal operation condition, the tubesheet temperature is uniform on the moderator side, as shown in Fig. 2 (b). But, in contrast to the normal operation condition, the fueling tubesheet is hotter than the moderator tubesheet, with a maximum temperature of 96°C at the top.

Finally, it should be emphasized that the original treatment of wall heat transfer in CFX-4, Eq. (2), does not take porous media into consideration. Its dependence on the turbulent kinetic energy, *k*, can have a significant implication to the wall heat transfer. For example, in the event of loss-of- forced circulation, the use of Eq. (2) yields a $h_w$ varying between 118 to 130 [W $m^{-2}$ $K^{-1}$]. This small $h_w$ leads to an extremely high tubesheet temperature
(> 200 $^0$C) on the fueling side, which is obviously wrong.

## 6. Conclusion

End-shield cooling effects under both normal and accidental conditions have been analyzed, using CFX-4 with an improved treatment of heat transfer between the wall and the cooling fluid when a porous medium is modeled. Because of the large hydraulic resistance of the porous medium, there is no flow recirculation simulated inside the end shield, and the flow is fairly uniform The simulated three-dimensional heat transfer agrees with the design specifications under normal operation conditions. Under loss-of-forced- flow condition, the model predicts a maximum tubesheet temperature of 96 °C, which is far below the coolant boiling temperature of 143 °C. The detailed temperature distribution simulated with the three-dimensional code can be used as input for stress analysis.

## 7. References

CFX 4.1 Flow solver, User Guide (1996). AEA technology.

Dixon, A. G. and Cresswell, D.L. (1979). "Theoretical prediction of effective heat transfer in packed bed", AIChe Journal, **25**, 663 - 676.

Kaviany, M. (1995). "Principles of Heat Transfer in Porous Media". Second Edition, Springer.

Yagi, S. and Wakao, N. (1959). "Heat and mass transfer from wall to fluid in packed beds", A.I.Ch.E. Journal, **5**, 79 - 85.

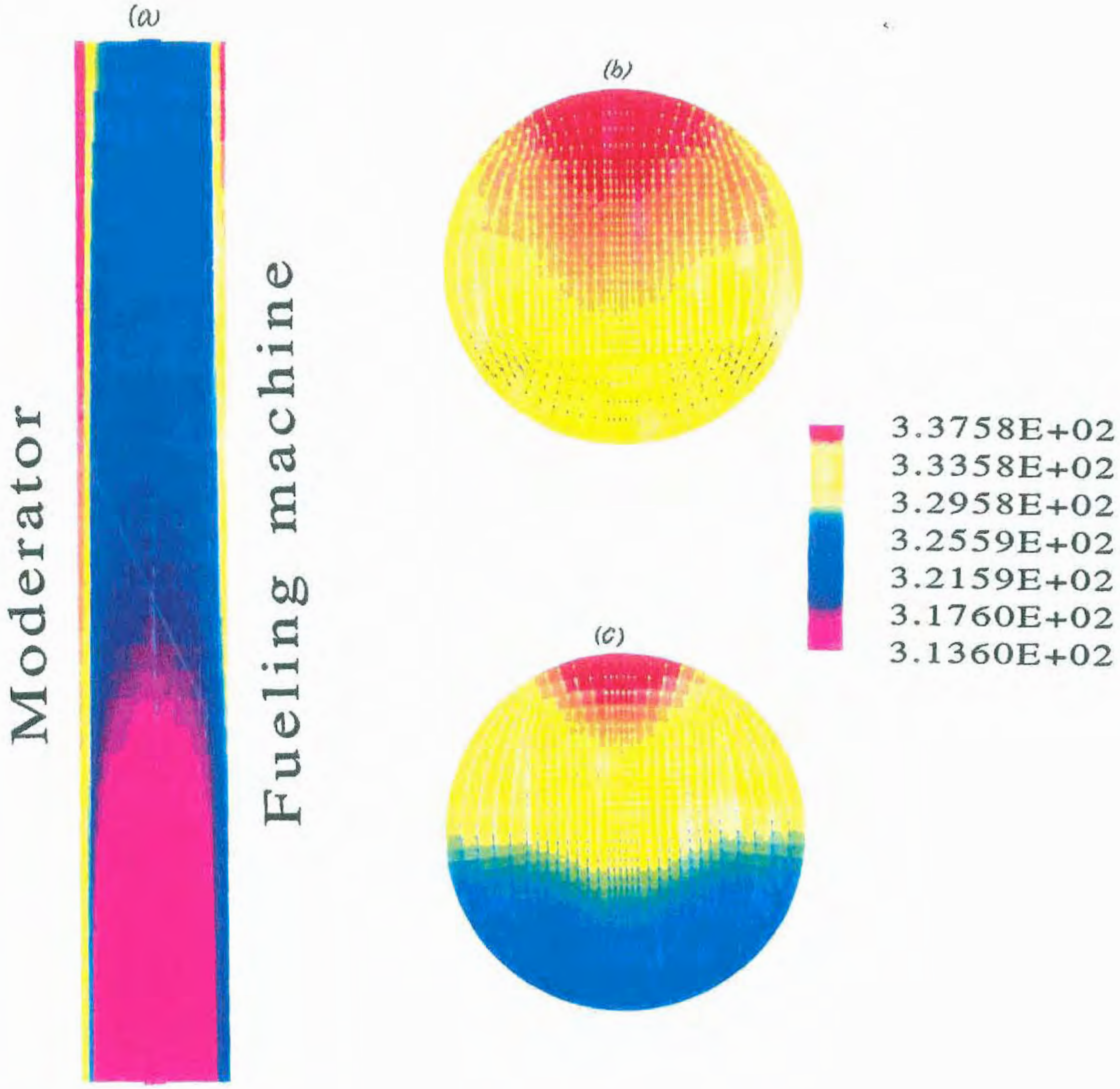


Figure 1. Temperature distributions of the end shield under normal operation conditions:
(a) side view, (b)on moderator side tubesheet and (c) on fueling tubesheet.

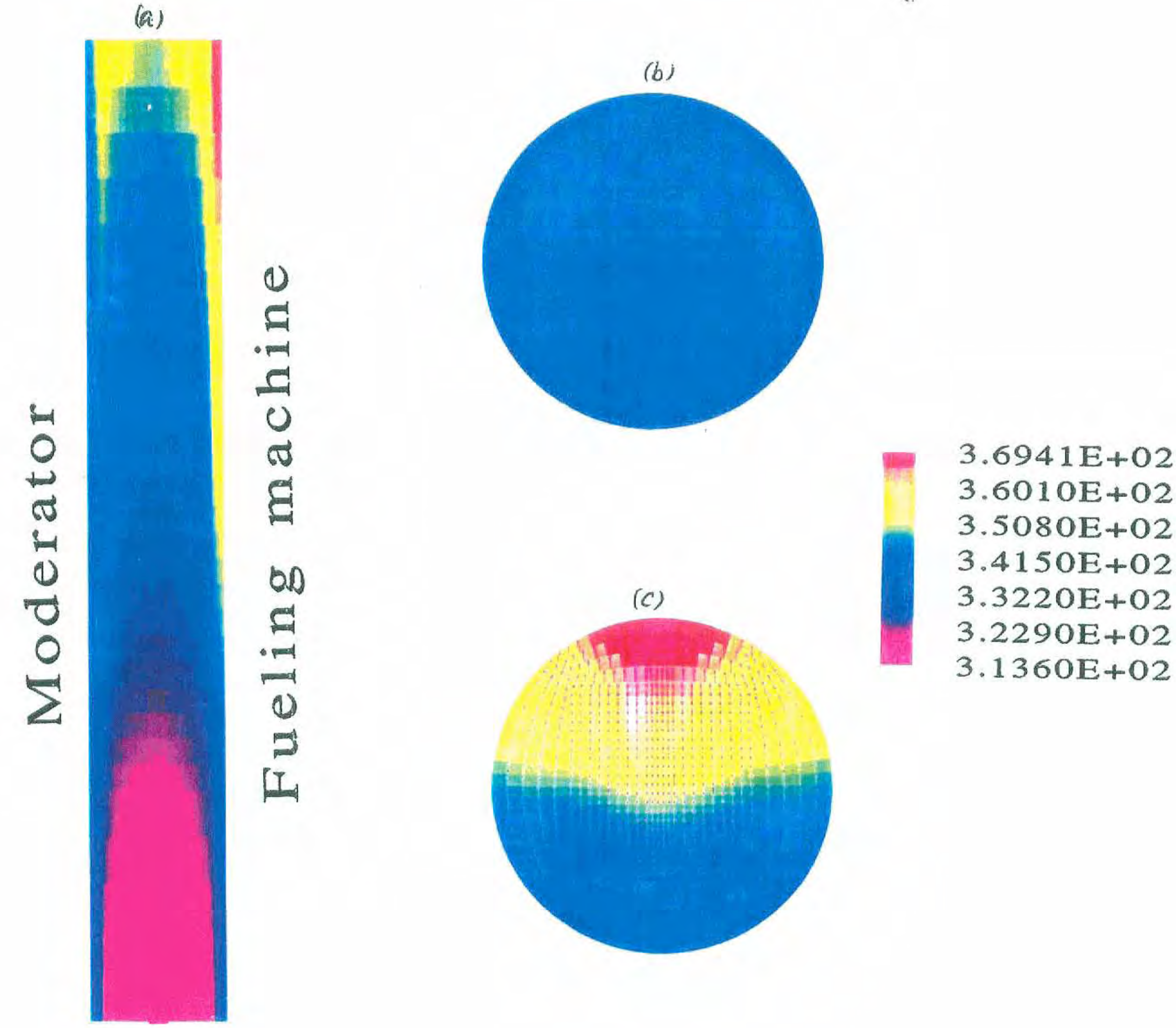


Figure 2. Temperature distributions of the end shield under loss of forced flow conditions: (a) side view, (b) on moderator side tubesheet and (c) on fueling tubesheet.